Journal of
Polymer Materials

Tech Science Press

Doi:10.32604/jpm.2025.063324

ARTICLE

Mechanical Properties and Fracture Behavior of 3D Printed Continuous Glass Fiber Reinforced PEEK Composite

Haoliang Ding[1,2], Han Yu[2], Yunfeng Zhao[2], Chunze Yan[1], Yusheng Shi[1,*] and Binling Chen[3,*]

[1]School of Materials Science and Engineering, Huazhong University of Science and Technology, Wuhan, 430074, China
[2]Aerospace Research Institute of Materials & Processing Technology, Beijing, 100076, China
[3]School of Mechanical Engineering, Beijing Institute of Technology, Beijing, 100081, China

*Corresponding Authors: Yusheng Shi. Email: shiyusheng@hust.edu.cn; Binling Chen. Email: chenbl@bit.edu.cn

Received: 11 January 2025; Accepted: 14 May 2025; Published: 11 July 2025

ABSTRACT: Polyether ether ketone (PEEK)-based continuous glass fiber reinforced thermoplastic composite offers advantages such as high strength, electrical insulation, and heat insulation. Parts manufactured using this composite and 3D printing have promising applications in aerospace, automobile, rail transit, etc. In this paper, a high-temperature melt impregnation method was used to successfully prepare the 3D printing prepreg filaments of the aforementioned composite. In the FDM 3D printing equipment, a nozzle of high thermal conductivity and wear-resistant copper alloy and a PEEK-based carbon fiber thermoplastic composite build plate with uniform temperature control were innovatively introduced to effectively improve the quality of 3D printing. The porosity of the 3D printed samples produced from the composite prepreg filament was analyzed under different printing parameters, and the mechanical properties and fracture mechanism of the printed parts were studied. The results show that the printing layer thickness, printing speed, printing temperature and build plate temperature have varying effects on the porosity of printed parts, which in turn affects tensile strength and the interlaminar shear strength (ILSS). When the printing layer thickness is 0.4 mm, printing speed is 2 mm/s, nozzle temperature is 430°C and build plate temperature is 150°C, the tensile strength and ILSS of the composite printed parts reach their maximum values of 463.76 and 24.95 MPa, respectively. Microscopic analysis of the fracture morphology of the tensile specimens reveals that the 3D printed CGF/PEEK composite sample has three types of fracture mode, which are single filament bundle fracture, fracture mode of delamination, and fracture failure of the sample at the cross-section. The essence of the above three kinds of fracture mode is the difference of the interface bonding force of 3D printed CGF/PEEK composites. The fracture failure at the cross-section is that the continuous glass fibers in the composite are pulled out until they break, which is the main form of the failure of the composite under tensile load. The interfacial region of the composite is prone to microscopic defects such as voids and delamination during 3D printing, which become the most vulnerable link of the composite. Understanding the relationship between voids and fracture behavior lays a foundation for defect suppression and performance improvement of subsequent printed parts.

KEYWORDS: 3D printing; continuous glass fiber reinforced PEEK composite; porosity; mechanical strength; fracture mechanism

1 Introduction

Continuous fiber reinforced thermoplastic composites (CFRTPCs) show great application prospects in aerospace, automobile, rail transit, and other industrial fields due to their high specific strength and modulus, good impact toughness, flexible and varied processability, recyclability and low energy consumption

[1–4]. Although CFRTPCs theoretically have the characteristics of high-temperature melting and repeated processing, it is very difficult for the recycling of CFRTPCs to maintain their continuous fiber state for reuse. Normally, CFRTPCs can only be used for secondary processing after the continuous fiber state is cut into the chopped fiber state by a crusher. Combining advanced 3D printing technology with CFRTPCs offers a promising method for designing and manufacturing of high-performance, low-cost complex structural parts. This technology bridges the gap between advanced materials and innovative structures [5]. Using polyether ether ketone (PEEK) as the matrix resin of CFRTPCs can further improve mechanical properties, heat resistance, corrosion resistance and adaptability to space environments [6–9].

A variety of reinforcements can be utilized in CFRTPCs, with common fiber-reinforced materials primarily including carbon fiber (CF), aramid fiber (AF), glass fiber (GF), ultra-high-molecular weight polyethylene (UHMWPE) fiber and basalt fiber (CBF) [10]. And CFRTPCs prepared from these fibers show different characteristics [11]. Among these CFRTPCs, continuous carbon fiber reinforced thermoplastic composites (CCFRTPCs) are a kind of well-documented and extensively studied composites, and their primary advantages include lightweight properties, high strength, and high modulus. Meanwhile, continuous aramid fiber-reinforced thermoplastic composites (CAFRTPCs) exhibit remarkable similarities to CCFRTPCs, and CAFRTPCs demonstrate good heat resistance, dimensional stability and energy absorption capabilities [12–14]. Besides, continuous glass fiber reinforced thermoplastic composites (CGFRTPCs) have the advantages of electrical insulation, thermal insulation, low dielectric properties and low cost [15–17].

Based on the specific application scenario, as well as the functional characteristics and processing quality of the required components, the aforementioned CFRTPCs were selected and fabricated via 3D printing technology. To manufacture 3D printed CGFRTPCs parts with high strength, electrical insulation, and thermal insulation properties, this study investigates the mechanical strength and fracture mechanisms of 3D printed PEEK-based CGFRTPCs. Additionally, this research establishes a foundation for further exploration of their electrical and thermal insulation characteristics.

The selection of a suitable 3D printing method for CFRTPCs is crucial to ensure the feasibility of printing the required components and to mitigate the defects in the printing process. The 3D printing methods of CFRTPCs mainly include *in-situ* impregnation printing and prepreg filament printing [18]. Prepreg filament printing can realize the initial impregnation of resin and continuous fiber during the preparation process, and then the secondary impregnation of filament can be further realized during the printing process, which is more suitable for the 3D printing of PEEK-based CGFRTPCs with high processing temperature and high melt viscosity.

However, for CGFRTPCs with PEEK as the matrix resin, the composite's good thermal insulation characteristic makes it difficult to fully melt the prepreg filament using an ordinary heating nozzle. Ordinary nozzles are usually made of hardened steel and traditional copper [19,20]. The higher glass fiber content and required printing speed further exacerbate the difficulty of full melting. In addition, the higher glass fiber content results in poor bonding between the composite material melt and the conventional steel base plate [21], coupled with the changes in the composite's shrinkage rate during cooling. This leads to the extruded melt from the nozzle not depositing well on the steel base plate, especially during the first layer deposition, causing failure in bonding with the build plate. To solve these problems, an improved nozzle made of high thermal conductivity (thermal conductivity of 330 W/m·K) and wear-resistant copper alloy (Mohs hardness of 6.0) was introduced to achieve efficient melting of the prepreg filament. In addition, a PEEK-based carbon fiber thermoplastic composite build plate was also developed, with a silicone rubber heater tightly attached to its back for uniform temperature control, enabling effective melting deposition and bonding of the prepreg filament's first layer on the build plate.

Due to the printing quality and mechanical properties of 3D printing PEEK-based CGFRTPCs, which are closely related to printing parameters, it is necessary to study the influence of different parameters. Printing parameters include printing layer thickness, printing speed, nozzle temperature, building plate temperature, chamber temperature, nozzle size, heat treatment method, etc. Yang et al. [22] discussed the relationship between various processing conditions (ambient temperature, nozzle temperature, heat treatment method) and the mechanical properties and crystallinity of PEEK. Wang et al. [23] reported the effects of nozzle diameter, printing speed, and nozzle temperature on the bending and compressive strength of PEEK samples. Zhi et al. [24] improved the printing precision by optimizing nozzle diameter, printing height, and printing speed. But, there are few reports on the effect of different printing parameters on porosity in the literature, especially for 3D printing PEEK-based CGFRTPCs.

Only a few literatures reported the relationship between porosity and fracture mechanism. Wang et al. [25] observed that no void defects were found on the fracture surface of PEEK samples due to the very high nozzle temperature (420°C). Dang et al. [26] studied the interlayer fracture properties of 3D-printed CFRTPCs, finding that the interlaminar failure of carbon fiber was seriously affected by the void defects caused by 3D-printed. Many literatures mainly study the fracture modes such as fiber debonding, fiber pull-out, surface fiber damage, matrix cracking and delamination failure. Zhang and Sun [27] analyzed the fracture failure modes of 3D printed continuous basalt fiber (CBF) reinforced thermoplastic composite products, mainly including fiber debonding, fiber pull-out, stress whitening, and matrix cracking, indicating that the fracture was mainly caused by the basalt fiber fracture. Li et al. [28] studied the failure mechanism of 3D printed CFRTPCs under quasi-static tensile load, including fiber bundle pull-out, fiber pull-out, fiber fracture, fiber/matrix debonding, and matrix brittle fracture. Liu et al. [29] showed failure modes such as fiber pull-out/breaking, matrix cracking, and delamination in fracture shear specimens through scanning electron microscopy (SEM) images. Parker et al. [30] noted that different degrees of fiber damage existed in CFRTPCs filament during different 3D printing stages, such as wire winding, wire feed wheel extrusion, nozzle extrusion, and printing deposition. Fiber damage near the surface of the filament resulted in fiber breakage during extrusion, with nozzle extrusion of and printing deposition causing the most harm. However, there are few literatures on the relationships between the fracture mode of single filament bundle fracture and delamination fracture and the regularity of void size and shape of 3D printing PEEK-based CGFRTPCs.

This paper analyzed the porosity characteristics of 3D printed PEEK-based CGFRTPCs samples under different printing parameters and studied the tensile strength and ILSS, as well as the fracture mechanisms. The relationship between the fracture mode and the void size and shape was revealed through the analysis of the microscopic morphology, which laid a foundation for defect suppression and performance improvement. The research results of this study are expected to apply the 3D-printed PEEK-based CGFRTPCs with high strength, electrical insulation and thermal insulation functions to aerospace, automotive, rail transit and other industrial fields in specific scenarios [31].

2 Materials and Methods

2.1 Raw Materials

PEEK Resin (ZYPEEK 310G), supplied by Jilin Zhongyan Polymer Materials Co., Ltd. (Changchun, China), is an unreinforced high melt index brand. High strength glass fiber twist roving (S6C11-300), supplied by Nanjing Glass Fiber Design Institute Co., Ltd. (Nanjing, China), is a kind of glass fiber yarn surface modified with thermoplastic sizing agent. The nominal diameter of the glass fiber is 11 μm, the linear density is 300 tex, and a single glass fiber bundle contains more than 1000 fibers. The mechanical properties of PEEK resin matrix and glass fiber are shown in Table 1, as provided by the above-mentioned manufacturers.

Table 1: Mechanical properties of the resin matrix and glass fiber

Mechanical properties	ZYPEEK 310G	S6C11-300
Density/g · cm^{-3}	1.3	2.5
Tensile strength/MPa	100*	≥3650
Modulus/GPa	4.3**	92.5
Elongation at break/%	25.0	–
Yarn strength/(N/tex)	–	≥0.65

Note: *Tensile yield strength; **Bending modulus.

2.2 Preparation of Continuous Fiber Composite Material Filaments

First, PEEK resin granules were dried at 150°C for 3 h to effectively remove the moisture on the resin. Then, continuous fiber composite materials were prepared using a self-made integrated extrusion equipment with melt impregnation (twin-screw diameter 20 mm, length-diameter ratio 40:1, traction roll diameter 80 mm). This equipment is designed and manufactured based on the high-temperature melt impregnation method. The high-temperature melt impregnation method is a method for the penetration of fibers by the molten thermoplastic resin. Since both permeation and diffusion are derived from concentration differences, they have some kinetic similarities. According to the theory of fluid mechanics and Darcy's law, the impregnation quality of fiber is related to many factors, such as physical parameters (number of fiber roots, diameter of fiber, thickness of fiber bundle, porosity, viscosity and flow rate, etc.), process parameters (traction speed, temperature and impregnation time, etc.) and mold structure parameters (number of rolls, diameter of rolls and coating Angle, etc.). The schematic diagram of the preparation equipment mentioned above is shown in Fig. 1. 3D printing continuous glass fiber reinforced PEEK composite filaments were prepared by impregnation and traction. During preparation, the traction line velocity was 0.5~4.0 mm/s, and the impregnation temperature was 370~390°C. The designed glass fiber mass content of the filaments was 35% ± 5%, and the filament diameter was controlled at 1.0 ± 0.1 mm. The cross-sectional morphology of the prepared filament is shown in Fig. 2. The glass fiber is relatively evenly distributed in the cross-section, and the glass fiber has good compatibility with PEEK resin, without obvious porosity defects.

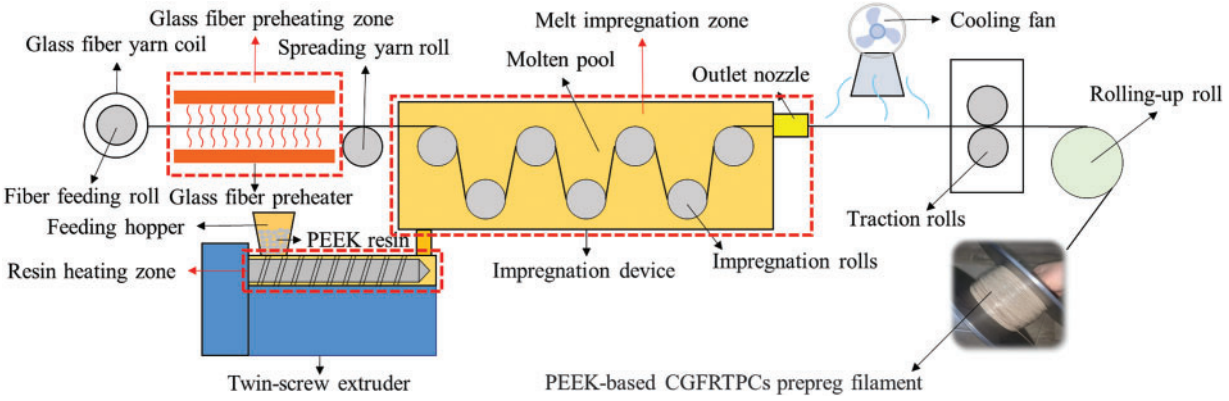

Figure 1: Schematic diagram of melt impregnation preparation equipment

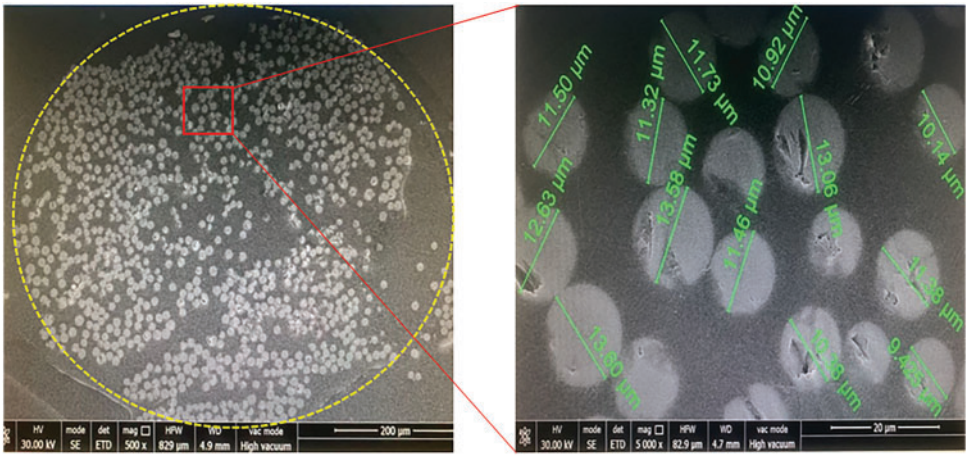

Figure 2: Cross section morphology of the prepared filament

2.3 3D Printing Device Design and Printing Settings

All the 3D printed samples in this paper were manufactured by the self-designed and modified FDM 3D printing device. The diagram of the enclosed print chamber of the FDM 3D printing device is shown in Fig. 3. To achieve efficient melting extrusion of PEEK-based CGFRTPCs prepreg filament, a nozzle made of high thermal conductivity and wear-resistant copper alloy was innovatively adopted. The copper alloy nozzle was specially customized with a Mohs hardness of 6.0, a thermal conductivity of 330 W/m · K and a maximum printing temperature of 500°C. The addition of tin in the copper alloy increased the hardness of the alloy and thus the wear resistance, while the addition of phosphorus also improved the wear resistance of the alloy. In addition, the nozzle was a flat-bottom nozzle, which had the effect of pressing the sediment layer during the printing process.

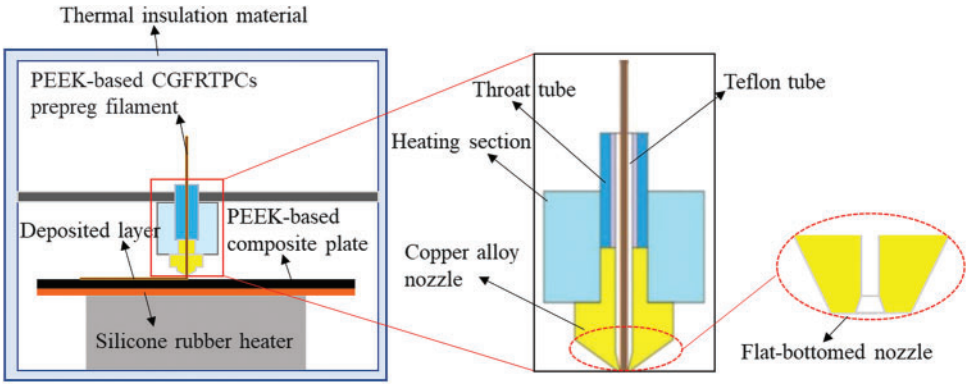

Figure 3: Diagram of enclosed print chamber of the FDM3D printing device

Besides, a PEEK-based carbon fiber thermoplastic composite build plate with uniform temperature control was constructed with a continuous carbon fiber reinforced PEEK(CCF/PEEK) plate as the base plate, and a silicone rubber heater was tightly attached to the back of the plate, so that heat could be uniformly transferred to the base plate, as shown in Fig. 4a. The carbon fiber mass content of CCF/PEEK plate was 63.2%, and the higher carbon fiber content made the plate have better thermal conductivity characteristics, which was conducive to heat transfer. The silicone rubber heater was composed of built-in heating elements,

an outer insulation layer sheet and temperature sensors, and the heater was shown in Fig. 4b. The internal heating elements were made of foils of nickel alloy, and their thermal power reached 1.2 W/cm^2, which could be evenly heated by uniform arrangement. The orange insulation layer sheet was made of silicone rubber and fiber cloth. The sheet had a certain softness and a thickness of 1.5 mm. The temperature sensors could timely and accurately feedback the temperature of the build plate, which was conducive to monitoring and controlling printing parameters. Under the effective control of build plate temperature, the adhesion between the deposition of CGF/PEEK composite and the build plate was greatly enhanced. The material of the build plate was similar to that of the prepreg filament, which facilitated better bonding of the deposited layer on the plate.

Figure 4: Physical images of 3D printing device. **(a)** PEEK-based composite plate (CCF/PEEK plate); **(b)** Silicone rubber heater

Tensile and interlaminar shear samples were modeled using CATIA V5 software and designed according to standard specifications. All the above 3D printed samples were set using the process parameters listed in Table 2, and none of the 3D printed samples underwent further heat treatment. The selection of the parameter range shown in Table 2 was determined by the test, especially by the porosity and appearance of the printed test sample. When the test porosity is less than 10%, the density of the printed test sample is generally higher, but if the porosity is too reduced, the processing efficiency will be sacrificed. In addition, the printing process also takes into account the appearance of the printed test sample. Print layer thickness and print speed were adjusted by simplify 3D software in the 3D printing device. Nozzle temperature, build plate temperature and chamber temperature were independently adjusted by temperature controllers in the printing device, and the accuracy of the controllers was ±1°C.

Table 2: Process parameters set for 3D printed samples

Parameters	State 1	State 2	State 3	State 4
Printing layer thickness/mm	0.4	0.5	0.6	0.7
Printing speed/(mm/s)	2	3	4	5
Nozzle temperature/°C	410	420	430	440

(Continued)

Table 2 (continued)

Parameters	State 1	State 2	State 3	State 4
Build plate temperature/°C	130	140	150	–
Chamber temperature/°C	150	150	150	150
Nozzle diameter/mm	1.2	1.2	1.2	1.2
Print path	0° straight path filling	0° straight path filling	0° straight path filling	0° straight path filling

2.4 Characterization of Mechanical Properties

The following tensile and interlaminar shear experimental conditions were tested using a universal machine (Instron5965) with a load capacity of 5 kN.

(1) The tensile property test was carried out according to the standard GB/T1447-2005, and the loading rate was 10 mm/min. The tensile sample was selected as the rectangular sample of type II in the standard, and its external size was set to 150 mm × 10 mm × 4 mm.

(2) The interlaminar shear performance was carried out according to the standard JC/T773-2010, the loading rate was 1 mm/min, the test span was 10 mm, and the external size of the interlayer shear performance sample was 20 mm × 10 mm × 2 mm. The ILSS was calculated by Formula (1).

$$\tau_w = \frac{3}{4} \times \frac{F}{b \cdot h} \tag{1}$$

where, τ_w was the ILSS, b and h were the width and thickness of the sample, and F was the failure load. Before the above mechanical properties test, the length and width of the sample section were measured 3 times each with a vernier caliper to obtain the average value. The test mechanical properties data were the average value of 5 repeated samples.

2.5 Characterization of Density and Porosity

The theoretical density ρ_c of the material sample was calculated by Formula (2).

$$\rho_c = \frac{\rho_f \cdot \rho_m}{\rho_f \left(1 - \omega_f\right) + \rho_m \cdot \omega_f} \tag{2}$$

where, ρ_m was the density of PEEK resin matrix, ρ_f was the density of fiber, ω_f was the mass fraction of fiber.

The use of multifunctional density instrument (AR-300VP, Shanghai Jingqi Instrument Co., Ltd., Shanghai, China) tested material sample actual density ρ using Formula (3) calculation.

$$\rho = \frac{m_1}{\left(m_1 - m_0\right)} \rho_s \tag{3}$$

where, m_1 was the mass of the material sample in air, m_0 was the mass of the material sample in water, ρ_s was the density of water, calculated according to $\rho_s = 1\ \mathrm{g/cm^3}$.

The porosity V_v of the material sample was calculated by Formula (4).

$$V_v = \frac{\rho_c - \rho}{\rho_c} \tag{4}$$

2.6 Characterization of Micromorphology

A scanning electron microscope (HITACHI S-4800, Japan HITACHI Co., Ltd., Tokyo, Japan) was used to observe the interlaminar fracture morphology of the material samples. Another scanning electron microscope (Quanta FEG650, USA FEI Co., Ltd., Hillsboro, OR, USA) observed the enlarged morphology of the cross section of the prepreg filament. Before the test, the sample with a 5 mm × 2 mm section size was first treated with brittle fracture under the condition of liquid nitrogen, and then the section surface of the observed sample was treated with gold spraying to observe the fracture microstructure of the section. A stereo microscope (CSW-SY500-H200RZ/SZM, Shenzhen Koshihui Optical Instrument Co., Ltd., Shenzhen, China) was used to magnify 20 times to observe the adhesion of the matrix on the surface of the material sample, in order to study the impregnation state and filling effect between the resin matrix and the fiber interface in the material sample.

3 Results and Discussion

3.1 Porosity of 3D Printed CGF/PEEK Composites

The variation curve of porosity with different process parameters is shown in Fig. 5. It can be seen that the porosity increases with both the printing layer thickness and printing speed. The porosity corresponding to the printing speed is generally higher than that corresponding to the printing layer thickness. When the printing layer thickness is 0.4 mm, the porosity is 6.79%, which is the lowest among the parameters tested. When the printing speed is 2 mm/s, the porosity is 8.48%, but at 5 mm/s, it reaches 27.45%, the highest observed, indicating that the printing speed has the most significant influence on porosity.

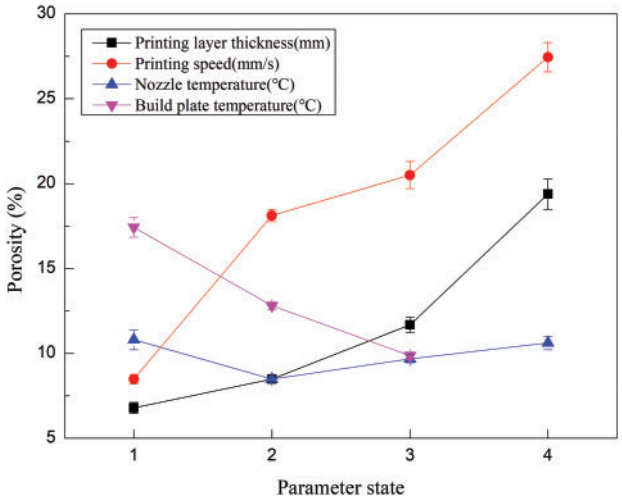

Figure 5: Variation curves of porosity with different process parameters

The reason for this phenomenon is that at higher printing speeds, the limited time in the nozzle leads to incomplete melting of the PEEK resin in the prepreg filament. Additionally, the low thermal conductivity and high glass fiber content exacerbate poor extrusion flow of the PEEK resin melt. This results in insufficient

filling between deposition lines within the same layer and inadequate compaction between layers, leading to more and larger voids, as shown in Fig. 6a,b. When the printing layer thickness is small, the molten prepreg filament deposited on the build plate experiences significant extrusion pressure from the flat-bottomed nozzle. The flat-bottomed nozzle increases the edge width of the bottom of the nozzle, which can increase the pressure during the printing process. It is beneficial to penetrate the molten PEEK resin matrix more evenly into the glass fiber bundles and between the adjacent deposition lines, and to improve the mechanical properties of the composites. In addition, increasing the edge width of the bottom of the nozzle can also increase the contact area between the nozzle and the deposit layer during the printing process. This is also conducive to the heat transfer of the nozzle heat between the deposited layers, further increasing the bonding of PEEK resin matrix between the deposition layers, and improving the density of the composites.

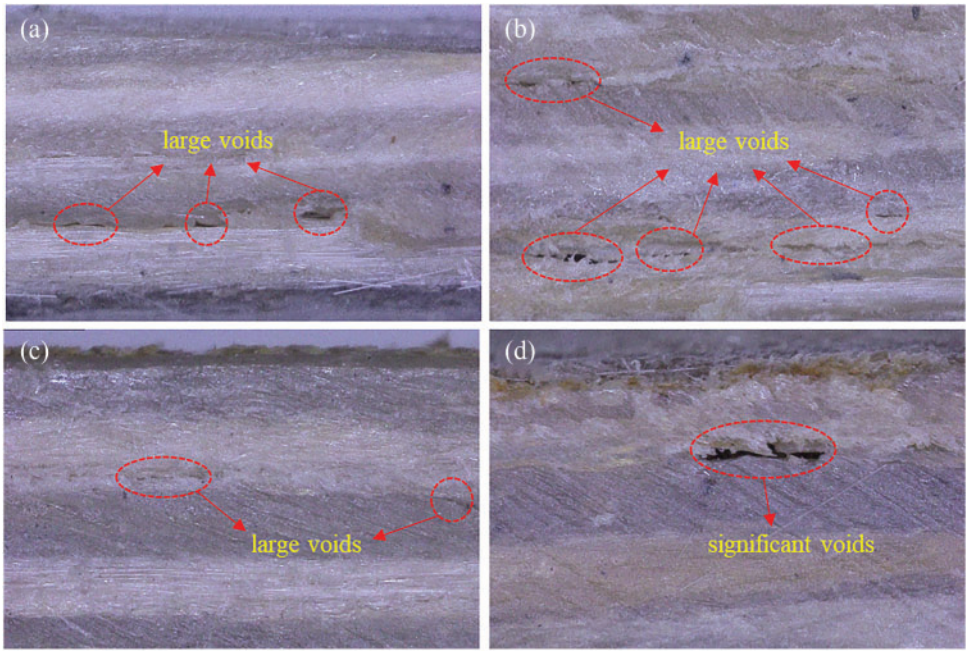

Figure 6: Microscopical photographs of the specimen layers at higher printing speed and larger printing layers thickness. **(a)** 4 mm/s (State 3); **(b)** 5 mm/s (State 4); **(c)** 0.6 mm (State 3); **(d)** 0.7 mm (State 4)

As the printing layer thickness increases, the extrusion pressure decreases, reducing the compaction effect between the layers and resulting in more and larger voids, as shown in Fig. 6c,d.

With the increase in nozzle temperature, the porosity slightly decreases initially and then gradually increases. When nozzle temperature is 420°C, the porosity is at low of 8.48%. Increasing the nozzle temperature from 410°C to 420°C reduces the viscosity of PEEK melt, improving the extrusion flow. However, further increasing the nozzle temperature to 440°C extends the cooling time of the deposited layers causing significant warping due to longer cooling processes. This warping results in large shrinkage stresses between layers, increasing voids and even causing delamination, as shown in Fig. 7.

In addition, porosity decreases with an increase in the build plate temperature. When the temperature of the build plate is 150°C, the porosity is reduced to 9.86%. A higher build plate temperature promotes the cooling crystallization of PEEK polymer during the transition from molten deposition to solidification. Since the glass transition temperature (Tg) of PEEK is 143°C, maintaining a temperature above this allows the polymer chain segments to remain active, extending molecular arrangement and crystallization time,

thereby increasing the density of the deposited layer and reducing porosity. This is because the crystallization process of PEEK is sensitive to temperature, and there is a significant difference before and after Tg. The crystallinity of PEEK samples will increase with the increase of the build plate temperature [32].

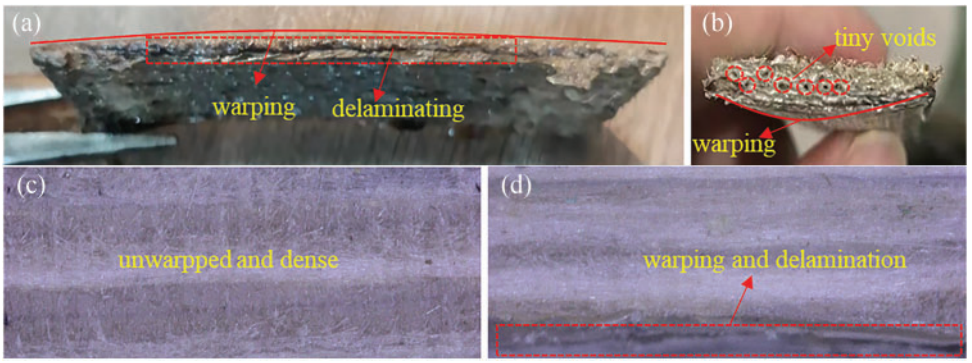

Figure 7: Photographs of sample edge at higher nozzle temperatures. **(a)** Length direction of printing (440°C); **(b)** Width direction of printing (440°C); **(c)** Enlarged images of sample edge (430°C); **(d)** Enlarged images of sample edge (440°C)

In summary, when the printing layer thickness is 0.4 mm, printing speed is 2 mm/s, nozzle temperature is 420°C, and build plate temperature is 150°C, the porosity of CGF/PEEK composite material is minimized.

3.2 Mechanical Strength of 3D Printed CGF/PEEK Composites

The variation curves of tensile strength and ILSS with different process parameters are shown in Fig. 8. It can be seen that both tensile strength and ILSS decrease with increasing printing layer thickness and printing speed. The mechanical strengths corresponding to printing speed are generally lower than those corresponding to the printing layer thickness, mainly due to the higher porosity discussed earlier. When the printing layer thickness is 0.4 mm, the porosity is 6.79%, resulting in a tensile strength of 449.56 MPa and an ILSS of 24.98 MPa. These values are higher than those at a printing speed of 2 mm/s. In terms of tensile strength, Kumekawa et al. [33] used continuous carbon fiber/nylon composite filament (measured diameter 0.359 ± 0.012 mm, Markforged), whose single layer thickness was smaller, only 0.15 mm. However, the tensile strength of optimized fiber path and layer thickness was only more than 160 MPa, which was lower than the results obtained in this study. In addition, Vatandas et al. [34] used 6K carbon fiber bundles (the diameter of carbon fiber is about 7 μm) to prepare continuous carbon fiber reinforced polylactic acid composite filament for 3D printing. The printing layer thickness of 6K CFRTP samples was 0.3 mm, and the tensile strength and ILSS of the samples were 653 and 11.44 MPa, respectively. The tensile strength was higher than that in this study because of the significant effect of carbon fiber reinforcement, but the ILSS was much lower than that in this study of 24.98 MPa, because of a weak bond between layers during the printing process. The poor bonding might be caused by nonhomogeneous mixture of the polylactic acid resin matrix and the carbon fiber, non-wetted carbon fibers, and porosities created by the printing process. In this study, PEEK resin has good compatibility with glass fiber, and better control of the porosity in the printing process.

Tensile and ILSS first increase and then decrease with the increase of the nozzle temperature, closely related to porosity changes. At a nozzle temperature of 430°C, its porosity is 9.68%, not the lowest compared to 8.48% at 420°C. However, a moderate increase of 10°C in nozzle temperature reduces the viscosity of the PEEK melt, improving flow and partially offsetting the negative impact of porosity on mechanical strength. At 430°C, the tensile strength reaches 463.76 MPa, and the ILSS is 24.95 MPa, the highest among

the tested parameters. However, the ILSS of CCF/PEEK composites mentioned in the literature has higher results than that of CGF/PEEK composites in this study. Luo et al. [35] improved the interlayer shear strength of CCF/PEEK composites through plasma-laser collaborative treatment. Among them, the laser treatment could improve the bonding between the printing layers and the crystallinity of the material, and the optimized ILSS of the sample reached 39.05 MPa. This data is significantly higher than that of 24.95 MPa in this study, which indicates that the addition of external facilities of the 3D printing device is an effective measure to further improve the mechanical properties of the composites.

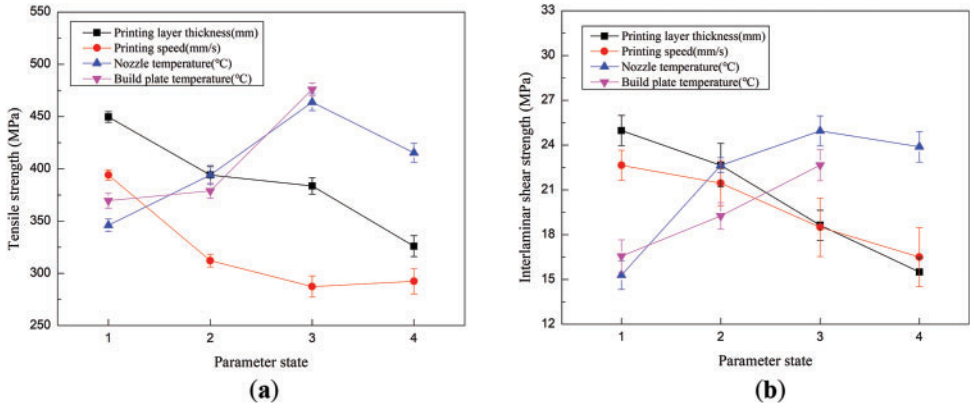

Figure 8: Variation curves of mechanical strength with different process parameters. **(a)**Tensile strength; **(b)** ILSS

Moreover, there is no warping between the layers of the sample and it is dense at this temperature, as shown in Fig. 7c. At 440°C, increased shrinkage stress due to warping between layers leads to more voids and delamination, as shown in Fig. 7a,b,d, as well as a decrease in mechanical strength. Both tensile strength and ILSS increase with the build plate temperature. At 150°C, the tensile strength is 475.94 MPa, and the ILSS is 22.65 MPa, higher than at 130°C and 140°C. The reason for this change is mainly related to the cooling crystallization of PEEK resin.

These mechanical strength variations align with the porosity trends under different process parameters, indicating that mechanical strength is mainly affected by porosity generated during 3D printing, lower porosity corresponds to higher mechanical strength. In addition, appropriately increasing the nozzle and build plate temperatures is helpful to improve the extrusion flow of PEEK resin melt and the cooling crystallization of PEEK resin. As a summary, when the printing layer thickness is 0.4 mm, printing speed is 2 mm/s, nozzle temperature is 430°C, and build plate temperature is 150°C, the tensile strength and ILSS of the CGF/PEEK composite material reach optimal and maximum values, namely 463.76 and 24.95 MPa. Liu et al. [17] designed and manufactured a stepped filament preparation mold, and used 600 tex continuous glass fiber yarn (Owens-Corning SE1200) to prepare CGF/PEEK composite filament, among which the glass fiber volume fraction of the filament prepared by the 0.8 mm mold was 48.454%. The tensile strength of the printed sample was as high as 730.21 MPa, and the ILSS was 39.15 MPa. These data are higher than those in this study, on the one hand, because of its high linear density of continuous glass fiber (600 tex), large numbers of single fiber bundle (1200), high glass fiber mass content of the filaments estimated (more than 70%), and small filament diameter (0.8 mm). On the other hand, the calculated porosity of the sample printed by an improved 3D printer with double-stage heating is low (1.237%), and the printing speed is also low (1.0~1.5 mm/s).

Compare our results with the mechanical strength of other published 3D printed PEEK-based CFRTPCS, as shown in Table 3. In terms of fiber content, after converting the volume content to the mass content, it is found that the fiber mass content reported in the literature is all relatively high, especially Liu et al. [15,17]. The fiber mass content can reach 59.4%. A higher fiber mass content inevitably leads to a greater viscosity of the melt at high temperatures, which causes a sharp increase in the difficulty of the 3D printing process. The fiber mass content in this study is only 35%, and the 3D printing forming process is less difficult, which is conducive to subsequent engineering applications. This is one of the advantages of this study. In terms of the diameter of pre-impregnated prepreg filaments, except for unidirectional pre-impregnated materials, the diameters of pre-impregnated prepreg filament reported in the literature are all less than 1 mm. Especially CCF/PEEK pre-impregnated wires are ultra-fine wire materials, but they are not suitable for preparation by high-temperature melt impregnation method, because they are prone to breakage during impregnation and traction. For CGF/PEEK prepreg filament, Liu et al. [17] pointed out that in terms of pore distribution, except for the 1.0 mm prepreg filament, there are certain voids inside the prepreg filament of other diameters, and when the diameter is reduced to 0.85 or 0.8 mm, the fibers tend to concentrate on the contour line of the prepreg filament. The diameter of the pre-impregnated prepreg filament in this study is 1 mm. On the one hand, it maintains a good roundness of the CGF/PEEK pre-impregnated prepreg filament. On the other hand, the glass fiber has good compatibility with PEEK resin and no obvious void defects. This is another advantage of this study.

Table 3: Comparison of our results with the mechanical strength of other published 3D printed PEEK-based CFRTPCs

CFRTPCs type	Fiber content/%	Fiber bundle number	Filament diameter/mm	Tensile strength/MPa	ILSS/MPa	Research characteristics	Year of publication	References
CGF/PEEK	35 (by mass)	1000	1.0	463.76	24.95	A modified nozzle structure and the composite base-plate	–	This study
CGF/PEEK	48.454 (by volume)	1000	0.80	730.21	39.15	A stepped filament preparation die	2024	Liu et al. [17]
CGF/PEEK	33.24 (by volume)	1000	0.94	524.33	46.28	A dual-stage heating nozzle with a preheating function	2022	Liu et al. [15]
CCF/PEEK	65~67 (by mass)	1000	0.40	–	21.24	A thermoplastic-based sizing treatment	2022	Qin et al. [36]
CCF/PEEK	42 (by volume)	3000	0.77~0.80	1312.0	35.1	Hot isostatic pressing (HIP) to post-process	2021	van de Werken et al. [37]
CCF/PEEK	59 (by volume)	3000	unidirectional prepregs	1513.8	–	Laser-assisted Laminated Object Manufacturing technique	2020	Chang et al. [38]
CCF/PEEK	–	1000	0.25	–	39.05	plasma-laser cooperatively assisted	2020	Luo et al. [35]
CCF/PEEK	38.27 (by mass)	1000	0.25	480*	35.7	Different laser preheating temperatures	2019	Luo et al. [39]

Note: *Flexural strength.

Although the results of this study in terms of mechanical strength are not as good as those reported in the literature, the 1 mm diameter CGF/PEEK pre-impregnated prepreg filament maintains good roundness, there are no obvious void defects inside the pre-impregnated prepreg filament, and its 3D printing process is less difficult, which has the advantages of better comprehensiveness.

3.3 Fracture Mechanism of 3D Printed CGF/PEEK Composites

SEM images of the cross-section of tensile specimens under different printing thicknesses are shown in Fig. 9. As the printing layer thickness increases, tiny voids in the cross-section of the tensile specimen gradually become larger voids, elliptical in shape and somewhat regular, eventually leading to connected voids and delamination. This trend is consistent with the increasing porosity described in Fig. 5. The progression from tiny to large voids and eventual delamination results in a significant decrease in mechanical strength, aligning with the trend of decreasing mechanical strength with increased printing layer thickness described in Fig. 8.

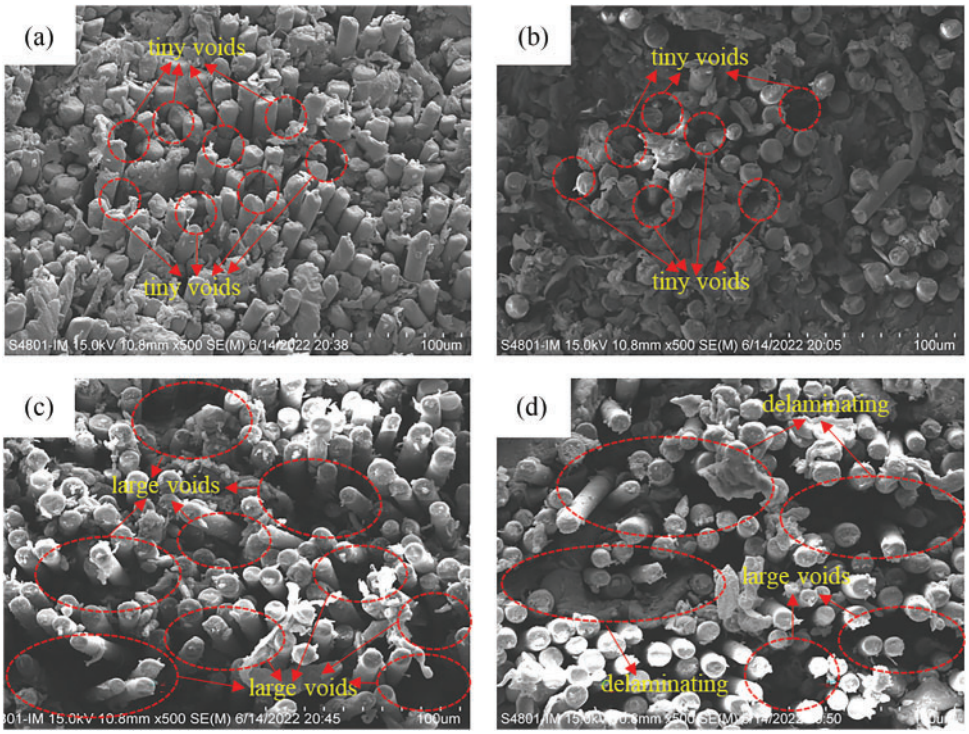

Figure 9: SEM cross-section photos of tensile specimens under different printing layer thickness. **(a)** 0.4 mm; **(b)** 0.5 mm; **(c)** 0.6 mm; **(d)** 0.7 mm

The fracture failure photographs of the sample before and after the tensile test are shown in Fig. 10. Compared with thermosetting composite tensile specimen prepared by conventional process such as molding, the tensile specimen of CFRTPCs prepared by 3D printing process has lower tensile strength due to some porosity (Section 3.2). During the tensile test, the sample was not easily pulled away from the fixture, and there was no significant stress concentration at the fixture that caused the sample to break at the fixture. Tensile fracture occurs mostly in the middle of the specimen, eliminating fixture influence. Therefore, tabs at both clamp edges of the sample used for this test were not utilized.

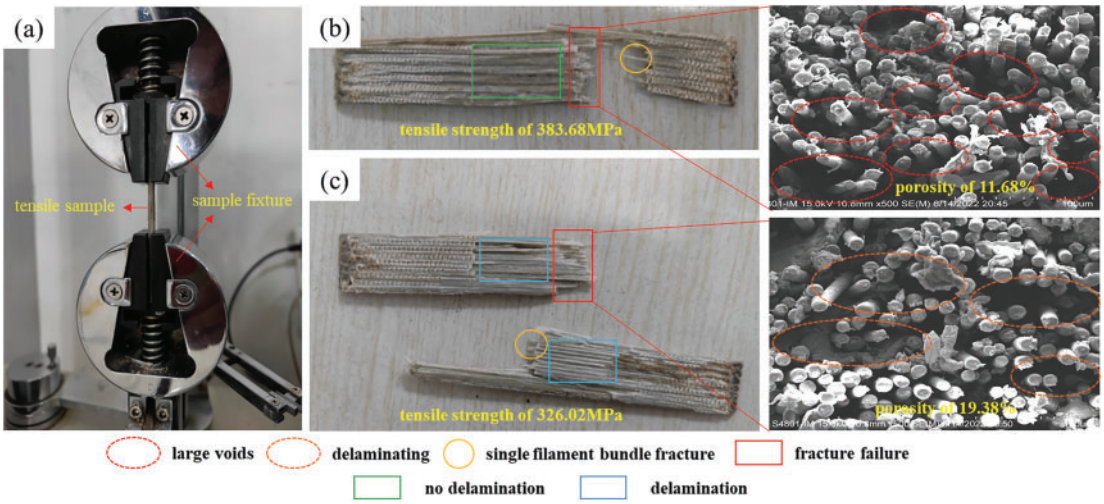

Figure 10: Fracture failure appearance of material samples before and after tensile test. **(a)** Before tensile test; **(b)** After tensile test (printing layer thickness 0.6 mm); **(c)** Specimen after tensile test (printing layer thickness 0.7 mm)

When the printing layer thickness is 0.6 mm, the sample shows two kinds of fracture mode after tensile test, one is single filament bundle fracture, and the other is the fracture failure of the sample at the cross section. Besides, there is no delamination failure on the surface and inside of the sample, and there are large voids at the cross section, as shown in Fig. 10b. Apart from the above two kinds of fracture mode, when printing layer thickness is 0.7 mm, the sample shows the third fracture mode of delamination after tensile test, and there are obvious delamination defects at the cross section, as shown in Fig. 10c. The essence of the above three kinds of fracture mode is the difference of the interface bonding force of 3D printed CGF/PEEK composites. Among them, the fracture of single filament bundle fracture originates from the damage of the interface of the interwire of 3D printing of CGF/PEEK composite filaments. The failure of interlayer delamination is mainly due to the failure of the bonding interface between deposition layers. The fracture failure at the cross section is that the continuous glass fibers in the composite are pulled out until they break, which is the main form of the failure of the composite under tensile load.

Good interfacial bonding force can prevent crack propagation and reduce stress concentration, but the interfacial region of the composite is prone to the above microscopic defects, such as voids and delamination during the preparation of prepreg filaments and 3D printing, which become the most vulnerable link of the composite. The surface of the continuous glass fiber yarn used in the preparation of PEEK-based CGFRTPCs in this study was treated with thermoplastic sizing agent, and there was no obvious void defects at the interface of glass fiber and PEEK resin in the prepreg filaments, as shown in Fig. 2.

Therefore, the defects of voids and delamination in Fig. 10 are mainly generated during 3D printing process. The diameter of prepreg filaments prepared in this study is 1 mm, and printing layer thickness is controlled by the distance between the bottom of the nozzle and the build plate. When the printing layer thickness is 0.4 mm, the molten prepreg filament is squeezed by the nozzle and form tiny voids. When the printing layer thickness increases to 0.6 mm and 0.7 mm, the contact pressure between the nozzle and the printing deposition is reduced, which can reduce the interface bonding force and compaction effect between printing depositions, resulting in the formation of large voids and even delamination at the interface between deposition layers. The shape of the voids is elliptical and has a certain regularity, and the porosity increases significantly (from 11.68% to 19.38%).

SEM images of tensile specimen cross-sections at different printing speeds and nozzle temperatures are shown in Figs. 11 and 12, respectively.

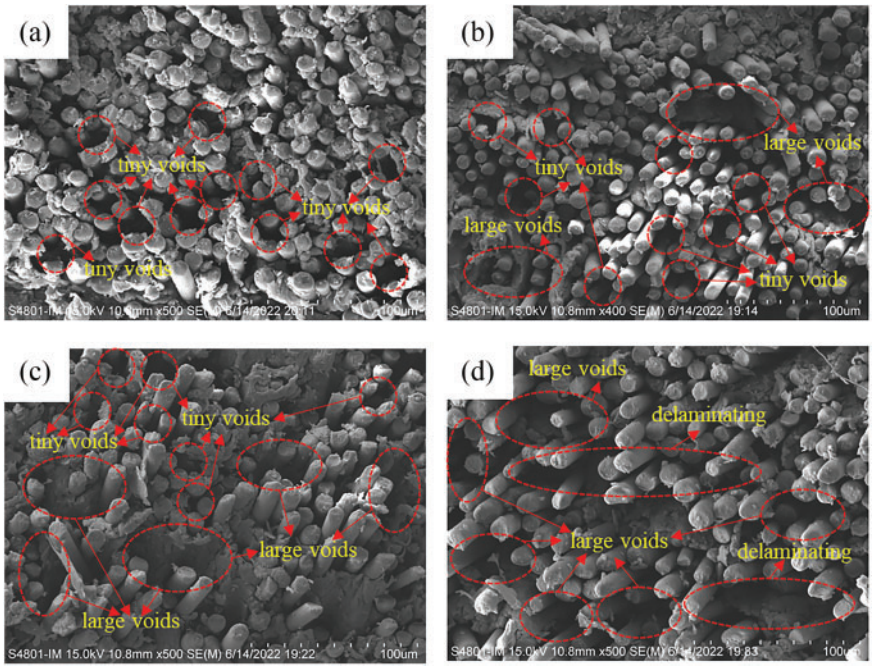

Figure 11: SEM photos of tensile specimen section at different printing speeds. **(a)** 2 mm/s; **(b)** 3 mm/s; **(c)** 4 mm/s; **(d)** 5 mm/s

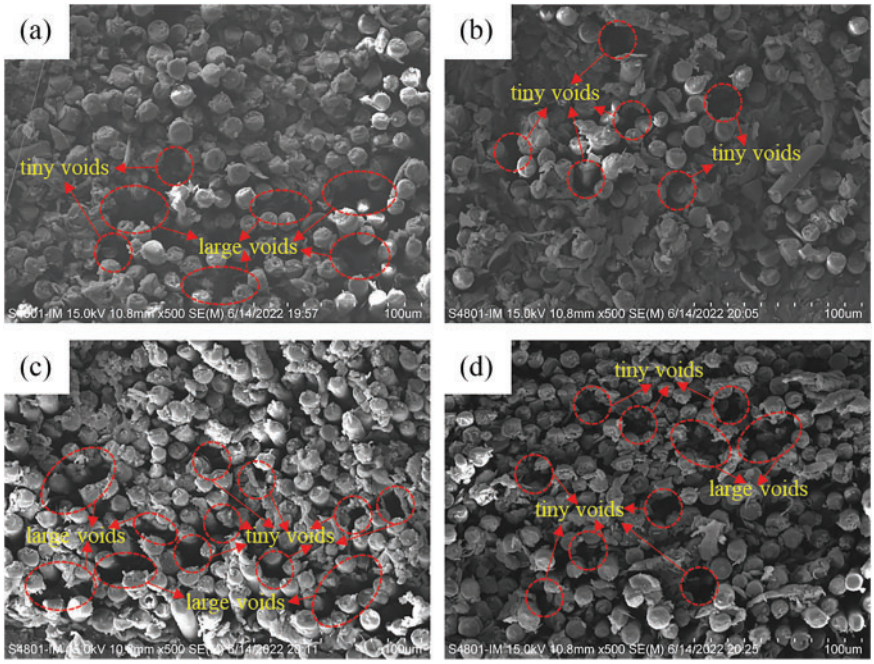

Figure 12: SEM photos of tensile specimen section at different nozzle temperatures. **(a)** 410°C; **(b)** 420°C; **(c)** 430°C; **(d)** 440°C

When printing speed reaches 4 mm/s and 5 mm/s, the sample section has obvious porosity and delamination defects. The defects produced at higher printing speeds are of varying sizes and irregular shapes, as shown in Fig. 11c,d. Printing speed is the speed at which the prepreg filament is pulled out of the nozzle, and the speed at which the nozzle moves on the build plate, which is controlled by the speed at which the nozzle moves.

Although the material of the nozzle is improved in this study, which is conducive to the melting of the prepreg filament, the length of the nozzle used in the experiment is shorter (13 mm), and the residence time of the prepreg filament in the nozzle is shortened from 6.5 s to 3.25 s and 2.6 s with the increase of the printing speed from 2 mm/s to 4 mm/s and 5 mm/s. This makes the PEEK resin matrix in the prepreg filament can not be melted in time, and the viscosity of the melt is higher, and the fluidity is poor. The melt with higher viscosity encounters greater resistance when flowing on the surface of the deposited layer, and it is difficult to penetrate into the surface of the deposited layer, and the infiltration effect is poor. Similarly, the melt of the higher viscosity also leads to poor infiltration between the wires.

Therefore, the faster printing speed causes the deterioration of melt infiltration effect, and the deterioration of infiltration produces voids and delamination defects at the interface between the wires and the layers of the printed deposition. The defects vary in size and shape, and the porosity increases significantly (from 20.50% to 27.45%), which is also larger than the porosity caused by a larger printing layer thickness.

It can be seen from Fig. 12 that with the increase of the nozzle temperature, the change of the cross-sectional voids of the tensile specimens is not obvious, with the tiny voids appearing at 420°C, consistent with the porosity changes described in Fig. 5. In addition, unlike the tensile specimen affected by printing layer thickness and printing speed, the fibers in the cross-sections influenced by nozzle temperature exhibit less pulled out, and the overall structure is relatively dense. This is because a moderate increase in nozzle temperature (from 410°C to 430°C) reduces the viscosity of the melt, improving flow and effectively mitigating the decline in mechanical strength due to porosity. This is also consistent with the trend of increased mechanical strength with higher nozzle temperatures described in Fig. 8.

No voids were observed on the fracture surface, and this could be attributed to a very high nozzle temperature (420°C) where polymer chains gain high energy and cause sufficient melting with increased fluidity of the filament. It also provides additional time for voids to get removed and, thereby increasing part density [25]. In addition, the higher nozzle temperature can increase the temperature of the deposited layer around the nozzle to reach the Tg of PEEK resin polymer, promote the movement of PEEK polymer molecular chain segments, improve the mutual diffusion degree of adjacent lines and interlayers PEEK resin molecular chains, and promote the fusion of deposited the wires and the layers interfaces.

4 Conclusion

In this paper, a nozzle structure of high thermal conductivity and wear-resistant copper alloy was introduced to achieve full melting of the prepreg wire, and a PEEK-based carbon fiber thermoplastic composite base-plate with uniform temperature control was also adopted to achieve deposition and bonding of the first layer of extruded melt. The nozzle structure and the composite base-plate were embedded into the self-designed and modified FDM 3D printing device, and then the porosity of the 3D printing sample produced by the composite prepreg wire was analyzed under different printing parameters, and the mechanical properties and fracture mechanism of the printed part were also studied. The following conclusions can be drawn:

(1) Printing layer thickness, printing speed, nozzle temperature and build plate temperature have different effects on the porosity of the printed parts, and the porosity further affects the tensile strength and

the ILSS. It basically shows that the porosity decreases, the forming density of the composite print increases, and the tensile strength and interlayer shear strength increase. Therefore, reducing porosity is an effective measure to improve the mechanical properties of composite materials. Specifically, the reduction of porosity is reflected in the optimization of the above parameters. With the decrease of printing layer thickness, printing speed and nozzle temperature and the increase of build plate temperature, the porosity tends to decrease.

(2) When the porosity is low, the corresponding process parameters are obviously relatively better processing windows. Specifically, under the condition of fixing other process parameters, the porosity of the printing layer is 6.79%, 8.48%, 8.48% and 9.86%, respectively, when the printing layer thickness, the printing speed, the printing nozzle temperature and the printing build plate temperature are 0.4 mm, 2 mm/s, 420°C and 150°C. In particular, when the nozzle temperature is 430°C, although the porosity is slightly as high as 9.68%, the tensile strength of the composite material is 463.76 MPa, and the ILSS is 24.95 MPa, and the overall mechanical properties are the best. Therefore, the optimal processing window is set as the thickness of the printing layer thickness 0.4 mm, the printing speed 2 mm/s, the printing nozzle temperature 430°C, and the printing build plate temperature 150°C.

(3) At a larger printing layer thickness (0.7 mm), the 3D printed CGF/PEEK composite sample has three types of fracture mode, which are single filament bundle fracture, fracture mode of delamination, and fracture failure of the sample at the cross section. The essence of the above three kinds of fracture mode is the difference in the interface bonding force of 3D printed CGF/PEEK composites. The fracture failure at the cross-section is that the continuous glass fibers in the composite are pulled out until they break, which is the main form of the failure of the composite under tensile load. The interfacial region of the composite is prone to microscopic defects such as voids and delamination during 3D printing, which become the most vulnerable link of the composite. The larger printing layer thickness (0.7 mm) leads to a decrease in the interface bonding force between the printing deposition layers, and the void defects have a certain regularity. The faster printing speed (4 mm/s and 5 mm/s) also results in different void sizes and irregular shapes. The faster printing speed also causes the infiltration effect of the melt to become worse, reducing the two kinds of interface bonding forces between the wires and the layers of the printed deposition layers. A moderate increase in nozzle temperature (from 410°C to 430°C) reduces the viscosity of the melt, improving the mutual diffusion degree of adjacent lines and interlayers PEEK resin molecular chains and promoting the fusion of deposited wires and the layers interfaces. The most significant degree of influence on the size and shape of the voids is the faster printing speed, followed by the thicker printing layer thickness, and the nozzle temperature is not obvious.

(4) This has laid the foundation for 3D printing high-quality manufacturing parts for aerospace, automotive, rail transit, etc.

Acknowledgement: The authors thank Dr. Mingyin Jia from Beijing University of Chemical Technology for his technical support in the material preparation method.

Funding Statement: This work was supported by the National Key Research and Development Program Project of China (Grant No. 2018YFB1106700).

Author Contributions: Conceptualization, methodology, writing—original draft preparation, Haoliang Ding; validation, data curation, investigation, Han Yu; writing—review and editing, Chunze Yan and Binling Chen; conceptualization, design, interpretation and funding acquisition, Yunfeng Zhao and Yusheng Shi. All authors reviewed the results and approved the final version of the manuscript.

Availability of Data and Materials: Data supporting the findings of this study will be made available on request.

Ethics Approval: Not applicable.

Conflicts of Interest: The authors declare no conflicts of interest to report regarding the present study.

References

1. Cheng P, Peng Y, Li S, Rao Y, Le Duigou A, Wang K, et al. 3D printed continuous fiber reinforced composite lightweight structures: a review and outlook. Compos Part B Eng. 2023;250:110450. doi:10.1016/j.compositesb.2022.110450.
2. Jandyal A, Chaturvedi I, Wazir I, Raina A, Ul Haq MI. 3D printing—a review of processes, materials and applications in Industry 4.0. Sustain Oper Comput. 2022;3(43):33–42. doi:10.1016/j.susoc.2021.09.004.
3. Ning F, Cong W, Qiu J, Wei J, Wang S. Additive manufacturing of carbon fiber reinforced thermoplastic composites using fused deposition modeling. Compos Part B Eng. 2015;80(1):369–78. doi:10.1016/j.compositesb.2015.06.013.
4. Zhang M, Tian X, Cao H, Liu T, Akmal Zia A, Li D. 3D printing of fully recyclable continuous fiber self-reinforced composites utilizing supercooled polymer melts. Compos Part A Appl Sci Manuf. 2023;169(10):107513. doi:10.1016/j.compositesa.2023.107513.
5. Tian X, Todoroki A, Liu T, Wu L, Hou Z, Ueda M, et al. 3D printing of continuous fiber reinforced polymer composites: development, application, and prospective. Chin J Mech Eng Addit Manuf Front. 2022;1(1):100016. doi:10.1016/j.cjmeam.2022.100016.
6. Kalra S, Munjal BS, Singh VR, Mahajan M, Bhattacharya B. Investigations on the suitability of PEEK material under space environment conditions and its application in a parabolic space antenna. Adv Space Res. 2019;63(12):4039–45. doi:10.1016/j.asr.2019.03.006.
7. Dai JN, Kou SQ, Yang HY, Xu ZB, Shu SL, Qiu F, et al. High-content continuous carbon fibers reinforced PEEK matrix composite with ultra-high mechanical and wear performance at elevated temperature. Compos Struct. 2022;295(8):115837. doi:10.1016/j.compstruct.2022.115837.
8. Ramaswamy K, Modi V, Rao PS, Martin PP, McCarthy CT, O'Higgins RM. An investigation of the influence of matrix properties and fibre-matrix interface behaviour on the mechanical performance of carbon fibre-reinforced PEKK and PEEK composites. Compos Part A Appl Sci Manuf. 2023;165:107359. doi:10.1016/j.compositesa.2022.107359.
9. Li Q, Zhao W, Li Y, Yang W, Wang G. Flexural properties and fracture behavior of CF/PEEK in orthogonal building orientation by FDM: microstructure and mechanism. Polymers. 2019;11(4):656. doi:10.3390/polym11040656.
10. Yang G, Park M, Park SJ. Recent progresses of fabrication and characterization of fibers-reinforced composites: a review. Compos Commun. 2019;14:34–42. doi:10.1016/j.coco.2019.05.004.
11. Dickson AN, Barry JN, McDonnell KA, Dowling DP. Fabrication of continuous carbon, glass and Kevlar fibre reinforced polymer composites using additive manufacturing. Addit Manuf. 2017;16(1):146–52. doi:10.1016/j.addma.2017.06.004.
12. Kukreja K, Panda PK. Aramid fiber, its composites and applications. In: Rangappa SM, Ayyappan V, Manik G, Siengchin S, editors. Synthetic and mineral fibers, their composites and applications. Amsterdam, The Netherlands: Elsevier; 2024. p. 61–99.
13. Huang Y, Tian X, Zheng Z, Li D, Malakhov AV, Polilov AN. Multiscale concurrent design and 3D printing of continuous fiber reinforced thermoplastic composites with optimized fiber trajectory and topological structure. Compos Struct. 2022;285:115241. doi:10.1016/j.compstruct.2022.115241.
14. Andres Leal A, Deitzel JM, McKnight SH, Gillespie JW. Interfacial behavior of high performance organic fibers. Polymer. 2009;50(5):1228–35. doi:10.1016/j.polymer.2009.01.018.
15. Liu X, Shan Z, Liu J, Xia H, Ao X, Zou A, et al. Mechanical and electrical properties of additive manufactured high-performance continuous glass fiber reinforced PEEK composites. Compos Part B Eng. 2022;247(1):110292. doi:10.1016/j.compositesb.2022.110292.
16. Chu XX, Wu ZX, Huang RJ, Zhou Y, Li LF. Mechanical and thermal expansion properties of glass fibers reinforced PEEK composites at cryogenic temperatures. Cryogenics. 2010;50(2):84–8. doi:10.1016/j.cryogenics.2009.12.003.

17. Liu X, Shan Z, Liu J, Liu F, Wu X, Zou A, et al. Mechanical and dielectric properties of continuous glass fiber reinforced poly-ether-ether-ketone composite components prepared by additive manufacturing. Addit Manuf. 2024;81(1):103978. doi:10.1016/j.addma.2024.103978.
18. Liu G, Xiong Y, Zhou L. Additive manufacturing of continuous fiber reinforced polymer composites: design opportunities and novel applications. Compos Commun. 2021;27:100907. doi:10.1016/j.coco.2021.100907.
19. Zhang P, Sun S, Duan J, Fu H, Han Z, Geng H, et al. Line width prediction and mechanical properties of 3D printed continuous fiber reinforced polypropylene composites. Addit Manuf. 2023;61:103372. doi:10.1016/j.addma.2022.103372.
20. Zhu W, Fu L, Zhi Q, Zhang Z, Wang N, Zhang Y, et al. Synergistic interlaminar strengthening of high-content continuous fiber reinforced composites via ultrasound and plasma-assisted 3D printing. Compos Sci Technol. 2025;263(2):111079. doi:10.1016/j.compscitech.2025.111079.
21. Shuto R, Norimatsu S, Arola DD, Matsuzaki R. Effect of the nozzle temperature on the microstructure and interlaminar strength in 3D printing of carbon fiber/polyphenylene sulfide composites. Compos Part C Open Access. 2022;9:100328. doi:10.1016/j.jcomc.2022.100328.
22. Yang C, Tian X, Li D, Cao Y, Zhao F, Shi C. Influence of thermal processing conditions in 3D printing on the crystallinity and mechanical properties of PEEK material. J Mater Process Technol. 2017;248:1–7. doi:10.1016/j.jmatprotec.2017.04.027.
23. Wang R, Cheng K, Advincula R, Chen Q. On the thermal processing and mechanical properties of 3D-printed polyether ether ketone. MRS Commun. 2019;9(3):1046–52. doi:10.1557/mrc.2019.86.
24. Zhi Q, Li D, Zhang Z, Fu L, Zhu W. High-content continuous carbon fiber reinforced multifunctional prepreg filaments suitable for direct 3D-printing. Compos Commun. 2023;44(1):101726. doi:10.1016/j.coco.2023.101726.
25. Wang P, Zou B, Xiao H, Ding S, Huang C. Effects of printing parameters of fused deposition modeling on mechanical properties, surface quality, and microstructure of PEEK. J Mater Process Technol. 2019;271(2):62–74. doi:10.1016/j.jmatprotec.2019.03.016.
26. Dang Z, Cao J, Pagani A, Zhang C. Fracture toughness determination and mechanism for mode-I interlaminar failure of 3D-printed carbon-Kevlar composites. Compos Commun. 2023;39:101532. doi:10.1016/j.coco.2023.101532.
27. Zhang H, Sun WF. Mechanical properties and failure behavior of 3D printed thermoplastic composites using continuous basalt fiber under high-volume fraction. Def Technol. 2023;27:237–50. doi:10.1016/j.dt.2022.07.010.
28. Li L, Liu W, Sun L. Mechanical characterization of 3D printed continuous carbon fiber reinforced thermoplastic composites. Compos Sci Technol. 2022;227(1):109618. doi:10.1016/j.compscitech.2022.109618.
29. Liu H, Zhou J, Kong X, Li S. Fracture behaviour of fibre-reinforced composite materials subjected to shear loading: an experimental and numerical study. Int J Lightweight Mater Manuf. 2023;6(1):108–16. doi:10.1016/j.ijlmm.2022.07.006.
30. Parker M, Ezeokeke N, Matsuzaki R, Arola D. Strength and its variability in 3D printing of polymer composites with continuous fibers. Mater Des. 2023;225(5):111505. doi:10.1016/j.matdes.2022.111505.
31. Ghnatios C, Fayazbakhsh K. Warping estimation of continuous fiber-reinforced composites made by robotic 3D printing. Addit Manuf. 2022;55(1):102796. doi:10.1016/j.addma.2022.102796.
32. Yu TP, Jiang XZ. Study on process parameters and crystallization behavior of polyetheretherketone in FDM printing. Mod Plast Process Appl. 2020;32(3):23–5. doi:10.19690/j.issn1004-3055.20190170.
33. Kumekawa N, Mori Y, Tanaka H, Matsuzaki R. Experimental evaluation of variable thickness 3D printing of continuous carbon fiber-reinforced composites. Compos Struct. 2022;288(3):115391. doi:10.1016/j.compstruct.2022.115391.
34. Vatandas BB, Usun A, Gumruk R, Simsek C. The relationship between fiber bundle size and mechanical performance of additively manufactured continuous carbon fiber reinforced thermoplastic composites. 3D Print Addit Manuf. 2023;10(6):1190–203. doi:10.1089/3dp.2022.0220.
35. Luo M, Tian X, Shang J, Yun J, Zhu W, Li D, et al. Bi-scale interfacial bond behaviors of CCF/PEEK composites by plasma-laser cooperatively assisted 3D printing process. Compos Part A Appl Sci Manuf. 2020;131(3):105812. doi:10.1016/j.compositesa.2020.105812.

36. Qin Y, Ge G, Yun J, Tian X, Liu X, Han J, et al. Enhanced impregnation behavior and interfacial bonding in CF/PEEK prepreg filaments for 3D printing application. J Mater Res Technol. 2022;20:4608–23. doi:10.1016/j.jmrt.2022.09.005.
37. van de Werken N, Koirala P, Ghorbani J, Doyle D, Tehrani M. Investigating the hot isostatic pressing of an additively manufactured continuous carbon fiber reinforced PEEK composite. Addit Manuf. 2021;37(1):101634. doi:10.1016/j.addma.2020.101634.
38. Chang B, Li X, Parandoush P, Ruan S, Shen C, Lin D. Additive manufacturing of continuous carbon fiber reinforced poly-ether-ether-ketone with ultrahigh mechanical properties. Polym Test. 2020;88:106563. doi:10.1016/j.polymertesting.2020.106563.
39. Luo M, Tian X, Shang J, Zhu W, Li D, Qin Y. Impregnation and interlayer bonding behaviours of 3D-printed continuous carbon-fiber-reinforced poly-ether-ether-ketone composites. Compos Part A Appl Sci Manuf. 2019;121(3):130–8. doi:10.1016/j.compositesa.2019.03.020.